

Trigonometric parallaxes of high velocity halo white dwarf candidates [★]

C. Ducourant¹, R. Teixeira^{2,1}, N.C. Hambly³, B. R. Oppenheimer⁴, M.R.S. Hawkins³, M. Rapaport¹, J. Modolo¹, and J.F. Lecampion¹

¹ Observatoire Aquitain des Sciences de l'Univers, CNRS-UMR 5804, BP 89, 33270 Floirac, France.

² Instituto de Astronomia, Geofísica e Ciências Atmosféricas, Universidade de São Paulo, Rua do Matão, 1226 - Cidade Universitária, 05508-900 São Paulo - SP, Brasil.

³ Scottish Universities Physics Alliance (SUPA), Institute for Astronomy, School of Physics, University of Edinburgh, Royal Observatory, Blackford Hill, Edinburgh, EH9 3HJ, UK.

⁴ Department of Astrophysics, American Museum of Natural History, 79th Street at Central Park West, New York, NY 10024-5192, USA.

Received / Accepted

ABSTRACT

Context. The status of 38 halo white dwarf candidates identified by Oppenheimer et al. (2001) has been intensively discussed by various authors. In analyses undertaken to date, trigonometric parallaxes are crucial missing data. Distance measurements are mandatory to kinematically segregate halo object from disk objects and hence enable a more reliable estimate of the local density of halo dark matter residing in such objects.

Aims. We present trigonometric parallax measurements for 15 candidate halo white dwarfs (WDs) selected from the Oppenheimer et al. (2001) list.

Methods. We observed the stars using the ESO 1.56-m Danish Telescope and ESO 2.2-m telescope from August 2001 to July 2004.

Results. Parallaxes with accuracies of 1–2 mas were determined yielding relative errors on distances of $\sim 5\%$ for 6 objects, $\sim 12\%$ for 3 objects, and $\sim 20\%$ for two more objects. Four stars appear to be too distant (probably farther than 100 pc) to have measurable parallaxes in our observations.

Conclusions. Distances, absolute magnitudes and revised space velocities were derived for the 15 halo WDs from the Oppenheimer et al. (2001) list. Halo membership is confirmed unambiguously for 6 objects while 5 objects may be thick disk members and 4 objects are too distant to draw any conclusion based solely on kinematics. Comparing our trigonometric parallaxes with photometric parallaxes used in previous work reveals an overestimation of distance as derived from photometric techniques. This new data set can be used to revise the halo white dwarf space density, and that analysis will be presented in a subsequent publication.

Key words. Astrometry : trigonometric parallax – Dark matter – Galaxy : halo – Star : kinematics – white dwarfs.

1. Introduction

In the last decade interest in the very cool, old white dwarf (WD) halo population has grown. This interest is motivated by the possibility that these objects could account for a significant fraction of the baryonic dark matter of our Galaxy. This idea is in accord with discussions attempting to explain the microlensing events in the Large Magellanic Cloud in terms of a halo WD population – see, for example, Chabrier et al. 1996 and Hansen 1998. Alcock et al. 1999 suggested that massive compact halo objects (MACHOs) make up 20 to 100% of the dark matter in the halo, with MACHOs having typical mass $m \sim 0.5 M_{\odot}$; more recently, Calchi Novati et al. 2005 find a similar result from pixel lensing in the line of sight to M31. Hence, in this scenario the search for, and direct study of, halo WDs can provide constraints on the fraction of dark matter in the Milk Way that is attributable to these objects.

Oppenheimer et al. (2001, hereafter OHDHS) identified 38 high proper motion WDs; from their kinematics, the authors

concluded that they were members of a halo population. Since then an intense discussion concerning the status of these objects has taken place in the literature. A comprehensive review of this debate is presented in Hansen and Liebert 2003 where the conclusion is that the OHDHS interpretation is possibly overstated, but that complete conclusions are not possible without further data. Other studies suggest that the disk and “thick disk” Galactic populations can be used to explain the great majority of the objects (Reid 2005, Kilic et al. 2005, Spagna et al. 2004, Crézé et al. 2004, Holopainen & Flynn 2004, Flynn et al. 2003, Silvestri et al. 2002). The importance of the high velocity WDs cannot be understated in other contexts (e.g. the star formation history of the Galaxy, see also Davies, King & Ritter 2002, Hansen 2003, Montiero et al. 2006). Moreover, several studies emphasise the importance of obtaining trigonometric parallaxes for candidate halo WDs (Bergeron & Leggett 2002, Torres et al. 2002, Bergeron 2003). This is especially important for the coolest WDs, whose spectral energy distributions show remarkable departures from black-body distributions and which are proving to be difficult to model accurately (Kowalski 2006, Gates et al. 2004, Saumon & Jacobson 1999, Hansen 1998). In the presence of such radical changes to the WD spectrum, the assumption of a monotonic photometric parallax relation (e.g. as

Send offprint requests to: ducourant@obs.u-bordeaux1.fr

[★] Based on observations collected at the European Southern Observatory, Chile (067.D-0107, 069.D-0054, 070.D-0028, 071.D-0005, 072.D-0153, 073.D-0028)

used in OHDHS) could break down and estimates of intrinsic space velocities could be in error seriously. Furthermore, a recent paper (Bergeron et al. 2005) concludes that precise distances are mandatory to derive accurate kinematics and ages for the putative halo WDs and in order to derive their evolutionary status.

Aiming to clear up this question, in 2001 we started an observing program with the ESO 1.56-m Danish and ESO 2.2-m telescopes to measure the trigonometric parallaxes of these stars. Trigonometric parallax measurements remain the only direct unbiased distance determination. They are of great importance in the debate about the status of cool halo white dwarfs because they are required to derive precise space velocities and ages which are used for distinguishing between halo and disk membership. These trigonometric parallaxes lead to the re-calibration of photometric distances used until now in this debate and allow analysis of the cool halo white dwarf population with more confidence. Unfortunately, due to limited observing time, only 15 stars on the OHDHS list have been observed to date. However, this sub-sample provides important insight into the problem.

2. Observations

Astrometric observations of 15 of the OHDHS list of 38 halo white dwarf candidates were performed at the ESO 2.2-m telescope equipped with the WFI wide-field mosaic camera (with $0.238''/\text{pixel}$, a field of view $\text{FOV} = 34' \times 33'$, 4×2 mosaic of $2k \times 4k$ CCDs), through the ESO 845 I filter. To reduce astrometric distortions and other instrumental effects, only data from chip 51 (with $\text{FOV} = 8' \times 16'$) were used in this work; target stars were centered in the FOV of this chip.

Four epochs of observation were acquired at maximum parallactic factor in Right Ascension in November 2002, July 2003, November 2003 and July 2004 with a total of 11 nights of observations. Two parallactic periods (four observations over 1.5 years) are required, at a minimum, for a unique determination of the parallax and proper motion. Two preliminary observing runs were performed at the ESO 1.56-m Danish telescope in July 2001 and July 2002 but the subsequent closure of the telescope forced the authors to move the program to the ESO 2.2-m telescope. Data acquired at the Danish telescope were not included in our final analysis to avoid systematic effects due to the use of two different telescopes.

To minimize differential colour refraction effects (DCR), observations were performed around the transit of targets with hour angles of less than 1 hour. Multiple exposures were taken at each observation epoch to reduce the astrometric errors and to estimate the precision of measurements. Exposure times varied from 100 to 600 seconds depending on the magnitude of the target. Each field was observed from 20 to 35 times.

3. Astrometric Reduction

3.1. Measurements

Frames were measured using the DAOPHOT II package (Stetson 1987), fitting a PSF. The significance level of a luminosity enhancement over the local sky brightness which was regarded as real was set to 7σ . The PSF routine was used to define a stellar point spread function for each frame. Finally we obtained the (x, y) measured positions, the internal magnitudes and associated errors of all stars on each frame. There were typically 300 to 600 stars measured on each frame depending on the exposure time. From these, a selection on the error in magnitude (ERRMAG)

as derived by the DAOPHOT II software was applied. Any observation with $\text{ERRMAG} \geq 0.15^m$ was rejected. Objects fainter than 1.5^m brighter than a given image's limiting magnitude were also rejected from the analysis.

3.2. Cross-Identification

For each of the 15 different fields of view, we selected a “master” or fiducial image from the set of 20 to 35 images. This master frame for each object had the deepest limiting magnitude and highest image quality. For each of the other images for a given target object, the positions of all stars not rejected by the criteria above were then cross-identified to the master image's star positions. Objects not detected on three or more frames were excluded, yielding 100 to 200 stars in common in each field. Frames containing less than $N_{\text{master}}/3$ stars in common with the master frame were removed from the solution (where N_{master} is the number of stars in the master frame). Note that the master frame is processed in an identical fashion to the other frames and is not assumed to be free of errors in the parallax solution. In other words, the fiducial frames are not taken as an error-free “truth”, but are simply used as a basis for coordinate transformations and correlation of star positions that comprise the astrometric grid used in the solution.

3.3. Differential Colour Refraction

Atmospheric refraction changes the apparent positions of stars in ground-based observations and depends on the zenith distance of the observations. For precision astrometry this effect must be accounted for, because it can be many tens of milliarcseconds at even relatively modest zenith distances. In our case, another effect becomes important as well, because the atmospheric refraction of our target stars will not be identical to that of the background stars used for our astrometric reference grid. Our target stars (WDs) and the background stars (typically main-sequence G or K stars) have different spectral energy distributions. Therefore, atmospheric refraction will affect them differently when observed through a given filter bandpass. This is called a differential colour refraction (DCR) and is known to cause spurious parallactic motion Monet et al. 1992. DCR can affect both the Right Ascension (RA) and Declination of the target as derived with respect to the field stars. Observations in parallax programs are planned to maximize the parallactic factor in RA so the parallax solution for the target will rely heavily on the RA measured. Therefore the parallax derived is mainly perturbed by the DCR effects in RA which are critically dependent on the zenith distance of a given observation.

We investigated the impact of such effects on the parallax of white dwarfs through simulations. Using the usual formula for atmospheric refraction, a blackbody approximation for white dwarf and background stellar spectra, the Besançon Galaxy model for background star characteristics (Robin et al. 1994) and ESO 845 filter limits, we computed the average differential colour refraction effects between a white dwarf similar to those of our list with effective temperatures, T_{eff} , in the range 4000 K to 11000 K (Bergeron et al. 2005, Table 2) and a typical background star ($T_{\text{eff}} \sim 5000$ K).

We present in Fig. 1 the effects of DCR in RA for white dwarfs situated at $\delta = -30^\circ$, covering the range of temperatures of our targets. Fig. 1 demonstrates that the impact of DCR effects were always less than 0.5 mas for observations taken with an hour angle of less than one hour. Therefore, our observations

were made specifically so that the hour angle never exceeded one hour, and DCR corrections were not applied in this work.

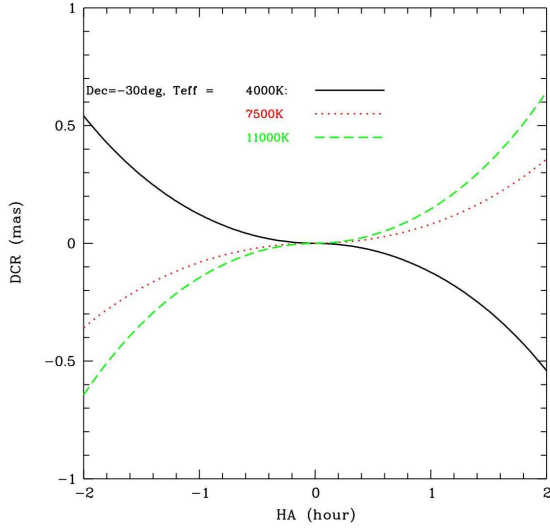


Fig. 1. DCR effects in RA between a white dwarf of temperature T_{eff} and a mean background stars ($T_{\text{eff}}=5000\text{K}$) at a Declination of -30° (representative of our sample) for various hour angles of observation. The DCR effects appear to be always lower than 0.5 mas for observations performed at less than 1 hour from meridian which is the case of the present project. The DCR effects are then negligible compared with other sources of astrometric error and were not taken into account in this work.

3.4. Impact of Pixel Scale Errors on Parallax

Proper motions (μ_x, μ_y) and trigonometric parallax (π_{xy}) of targets are determined by comparing the (x, y) measurements expressed in pixels. A scaling factor S_f , the image pixel scale, is applied to π_{xy} to convert pixel measurements into physical units: $\pi = S_f \pi_{xy}$; $d(\text{pc}) = \pi^{-1}$, with S_f expressed in $''/\text{pixel}$.

Derivation of the pixel scale can be achieved through a cross-correlation between the (x, y) positions of stars on a given master frame to corresponding values of (α, δ) for the subset of stars that are also in a reference catalogue. Here we used the 2MASS catalogue (Cutri et al. 2003) to determine the orientation of the master frame on the sky and for the pixel scale determination. We selected the 2MASS catalogue as a reference catalogue because of its accuracy and density although we note the absence of proper motion corrections. Nevertheless the epoch difference between our observations and the 2MASS catalogue (3 years) would result in negligible corrections to the catalogue positions with respect to the catalogue errors.

Errors on the scale so determined, resulting from catalogue random errors, will produce errors in the distance determination of the target. It is therefore important to quantify the impact of the catalogue errors onto the distance of the target.

To measure this impact in the present work, we assumed N reference stars equally spread over a square detector of side A . The classical equation relating the (x, y) measurements of a stars on the frame to its standard coordinates $X(\alpha, \delta), Y(\alpha, \delta)$ in the tangent plane to the celestial sphere is (with a similar equation in the Y coordinate)

$$X = (ax + by + c)1/F, \quad (1)$$

where (a, b, c) are the unknown “plate” constants and F the focal length of the telescope (typically the value indicated in the reference manual). F is expressed in the same units as (x, y) and A (pixel, mm). It is then easy to show that a fair approximation of the variance of the estimation of parameter (a) is given by

$$\sigma_a \sim \sqrt{\frac{12}{N}} \frac{F}{A} \epsilon_{\text{cat}}, \quad (2)$$

where ϵ_{cat} is the catalogue precision (expressed in radians). Similar results can be found in Eichhorn & Williams 1963. We can express the parallax (in radians) as:

$$\pi = \frac{a}{F} \pi_{xy}, \quad (3)$$

with

$$\sigma_\pi^2 = \pi_{xy}^2 \frac{1}{F^2} \sigma_a^2, \quad \sigma_\pi = \frac{\pi_{xy}}{F} \sqrt{\frac{12}{N}} \frac{F}{A} \epsilon_{\text{cat}} \quad (4)$$

with $F \sim 13\text{m}$, $A \sim 0.03\text{m}$, we evaluate here $\sigma_\pi \sim 10^{-4}\pi$. The impact of the error of the catalogue on the parallax of the target is far below the measurement errors (typically a few milliarcseconds) and are therefore negligible.

3.5. Global Solution: Relative Parallax

The astrometric reduction of the whole set of data of each field is performed iteratively through a global central overlap procedure (Hawkins et al. 1998, Eichhorn 1997) in order to determine simultaneously the position, the proper motion and the parallax of each object of the field.

The following condition equations are written for each star on each of the N frames considered (including the master frame). These equations relate the measured coordinates to the stellar astrometric parameters:

$$X_0 + \Delta X_0 + \mu_X(t - t_0) + \pi F_X(t) = a_1 x(t) + a_2 y(t) + a_3 \quad (5)$$

$$Y_0 + \Delta Y_0 + \mu_Y(t - t_0) + \pi F_Y(t) = b_1 x(t) + b_2 y(t) + b_3 \quad (6)$$

where (X_0, Y_0) are the known standard coordinate of the star at the epoch t_0 of the master frame, and $(x(t), y(t))$ its measured coordinates on the frame (epoch t) to be transformed into the master frame system. $\Delta X_0, \Delta Y_0, \mu_X, \mu_Y$ and π are the unknown stellar astrometric parameters: $(\Delta X_0, \Delta Y_0)$ yield correction of the standard coordinates of the star on the master frame, (μ_X, μ_Y) are the projected proper motion in RA $\ast \cos(\delta)$ and Dec, and π is the parallax. Coefficients (a_i, b_i) are the unknown frame parameters which describe the transformation to the master frame system. (F_X, F_Y) are the parallax factors in standard coordinates. The unknowns of this large over-determined system of equations are the stellar astrometric parameters of each object, and the transformation coefficients of each of the N frames considered. The system of equations is singular and therefore the derived solution is not unique; any solution will depend on the starting point of the iterations. The usual technique to obtain a particular solution is to introduce a set of constraints that the solution must satisfy. In this work we chose to set strictly to zero the mean parallax of the reference stars.

We used a Gauss–Seidel type iterative method to solve the set of equations. At the first iteration all stellar parameters are assumed null, we then computed the plate constants which are

injected into the system of equations to derive the stellar parameters. These results are then used as the starting point of the following iteration. The iterative procedure converges usually at the second or third iteration. A test of elimination at 3σ is applied to remove poor observations either in the master frame fit or in the stellar parameters fit. The stellar parameters fit equations have been weighted by the mean residual of the master frame fit. This weighting represents the quality of the measurements. The stars used for the master frame fit are called here reference stars.

We applied this global treatment to the various observations of the 15 fields observed and we derived for the targets a proper motion and parallax with associated variances.

3.6. Conversion from Relative to Absolute Parallax

The parallaxes that we derived for our targets are relative to the reference stars (for which we used the constraint $\sum \pi = 0$), supposed placed at infinite distance. In fact these reference stars are at a finite distance from Sun. We must therefore correct the relative parallax of the target from an estimate of the mean distance of the reference stars to obtain the absolute parallax of the target. The choice we made to keep as many reference stars as possible in our calculation is interesting because statistically faint stars have smaller parallax and require smaller correction.

There are several ways to estimate the mean distance of reference stars: statistical methods relying on a model of the Galaxy; spectroscopic parallax; and photometric parallax. For the corrections from relative parallax to absolute parallax we used a statistical method relying on simulations using the Besançon Galaxy model (Robin et al. 1994) to derive the theoretical mean distance of reference stars. A simulation of each observed field was performed, providing catalogues of distance and apparent magnitude of simulated stars. We computed in these catalogues mean distances and associated dispersion in magnitude bins of 0.2 mag, establishing a table of theoretical distances with respect to apparent magnitude. Then we considered our observed fields and we computed the weighted mean parallax and associated dispersion of our reference stars using the theoretical table. Finally we added this mean parallax of reference stars to the relative parallax of our target leading to the absolute parallax of the white dwarfs.

We give in Table 1 the relative to absolute corrections in milliarcseconds as found from the Besançon Galaxy model in each of the field treated.

4. Results

4.1. Distances of Halo White Dwarf Candidates

We present in Table 2 the proper motions and absolute parallaxes of the fifteen halo white dwarf candidates as derived from this work together with their absolute magnitude M_V computed using CCD V magnitudes from Bergeron et al. (2005).

One notices that WD2326–272, LP586–51, LP588–37, and WD2324–595 are too distant to have a measurable parallax. Eleven objects are at distances ranging from 19 pc to 90 pc from the Sun. The parallax errors are about 1–2 mas corresponding to relative precisions of 5 to 20%. WD2214–390, which is the closest and brightest object, has a $\sigma_\pi = 2.6$ mas. This poor precision is due to the short exposure time used to avoid saturation problems and corresponding lower signal-to-noise ratio.

We present in Figs 8 and ?? the positions (empty circles), their weighted mean (filled circles) and associated error bars at

Table 1. Relative to absolute corrections $\Delta\pi$ and associated RMS (σ) as found from the Besançon Galaxy model in the Galactic direction (l,b) together with number of reference stars (N^*) in magnitude interval $[J_{\min}, J_{\max}]$.

Target	l [°]	b [°]	$\Delta\pi$ [mas]	σ	N^*	J_{\min} [mag]	J_{\max} [mag]
WD2214-390	2.79	-55.37	1.3	0.3	38	13.1	16.2
WD2242-197	40.01	-59.42	1.0	0.3	97	14.0	18.4
WD2259-465	344.30	-60.62	1.1	0.2	83	13.6	18.0
LHS542	72.40	-59.70	1.2	0.3	42	13.4	17.0
WD2324-595	321.83	-54.34	1.1	0.2	62	13.3	17.0
WD2326-272	27.66	-71.06	1.3	0.4	80	14.2	18.7
LHS4033	90.24	-61.96	1.3	0.2	39	14.2	16.5
LHS4041	351.44	-74.66	1.4	0.3	37	13.5	16.2
LHS4042	6.55	-76.61	1.5	0.4	38	13.3	16.6
WD0045-061	118.54	-68.96	1.5	0.3	54	13.5	17.7
F351-50	314.26	-83.50	0.3	0.2	53	14.1	18.1
LP586-51	128.88	-63.30	1.3	0.3	47	14.1	17.4
WD0135-039	149.30	-64.53	1.3	0.2	82	14.4	19.0
LP588-37	150.44	-61.52	1.4	0.2	57	13.6	17.7
LHS147	178.72	-73.56	1.5	0.3	43	13.4	16.8

each epoch of observation, together with the fitted path for the eleven most significant parallaxes, where $\pi/\sigma_\pi \geq 4$.

4.2. Comparison with Published Distances

We have compared our results with available data from the literature, employing both trigonometric and photometric parallaxes measured previously. We give in Table 3 the comparison with published trigonometric parallaxes and in Figure 2 a comparison of the parallaxes derived in this work with photometric parallaxes (from OHDHS, where photometric parallax errors were 20%). Parameters of a weighted linear fit between photometric and trigonometric parallaxes are: $\pi_{\text{trig}} = a\pi_{\text{phot}} + b$ with $a = 1.08 \pm 0.08$ and $b = 3.21 \pm 1.56$ [mas] with a reduced $\chi^2 = 8.06$.

Table 3. Comparison of trigonometric parallaxes from this work (π_{Thiswork}) with published data (π_{ext}) for LHS 147 (Van Altena et al. 1995), LHS 4033 (Dahn et al. 2004) and LHS 542 (Bergeron et al. 2005).

Target	π_{Thiswork} [mas]	π_{ext} [mas]	$\Delta\pi$ [mas]
LHS 542	29.6 +/- 1.8	32.2 +/- 3.7	2.6
LHS 147	14.8 +/- 1.8	14.0 +/- 9.2	-0.8
LHS 4033	30.1 +/- 1.8	33.9 +/- 0.6	3.8

Our parallaxes are in excellent agreement with the 3 previously published trigonometric parallaxes, within the errors (which are considerably smaller in two cases than published values). In Fig. 2 one notices a clear systematic tendency of photometric parallaxes to be underestimated. This overestimation of OHDHS distances is of importance in the calculation of WD kinematics and space density.

Table 2. Proper motion and absolute parallaxes of the fifteen halo white dwarf candidates, where $\mu_{\alpha*} = \mu_{\alpha} \cos(\delta)$ and $\sigma_{\mu} = \sigma_{\mu_{\alpha*}} = \sigma_{\mu_{\delta}}$; π and σ_{π} are the parallax and its precision, Dist the derived distance in parsec and M_V the absolute magnitude. No value is given for Dist and M_V when the parallax is not better than 3σ . N* is the number of reference stars and Nf the Number of frames. D_{phot} is the photometric distance from OHDHS and V is extracted from Bergeron et al. (2005) when available, otherwise (cases marked by an asterix) it comes from Salim et al. (2004). Note that LHS 4041 is in the OHDHS sample, but is not listed in OHDHS Table 1 (see Table 4 of Salim et al. 2004)

Name	α [J2000]	δ	Epoch [yr]	V [mag]	$\mu_{\alpha*}$ [mas/yr]	μ_{δ} [mas/yr]	σ_{μ}	π [mas]	σ_{π}	Dist [pc]	M_V [mag]	N*	Nf	D_{phot} [pc]
WD2214–390	22 14 34.727	–38 59 07.05	2003.5	15.92	1009	–350	2.9	53.5	2.6	19	14.78	38	28	24
WD2242–197	22 41 44.252	–19 40 41.41	2003.5	19.74	359	+48	3.1	11.1	2.3	90	14.89	97	27	117
WD2259–465	22 59 06.633	–46 27 58.86	2002.9	19.56	402	–153	1.8	22.7	1.3	44	16.49	83	32	71
LHS542	23 19 09.518	–06 12 49.92	2003.5	18.15	–615	–1576	1.8	29.6	1.8	34	15.58	42	33	42
WD2324–595	23 24 10.165	–59 28 07.95	2003.5	16.79	136	–562	1.8	(3.1)	1.5	—	—	62	25	58
WD2326–272	23 26 10.718	–27 14 46.68	2002.9	*19.92	574	–85	2.7	(6.2)	2.4	—	—	80	17	108
LHS4033	23 52 31.941	–02 53 11.76	2002.9	16.98	631	298	2.5	30.1	1.8	33	14.38	39	26	63
LHS4041	23 54 18.793	–36 33 54.60	2002.9	*15.46	21	–662	1.8	13.4	1.5	75	11.10	37	27	59
LHS4042	23 54 35.034	–32 21 19.44	2003.5	17.41	421	–37	2.2	13.9	1.8	72	13.13	38	25	85
WD0045–061	00 45 06.325	–06 08 19.65	2002.9	18.26	111	–668	1.9	30.1	1.9	33	15.59	54	27	44
F351–50	00 45 19.695	–33 29 29.46	2003.5	19.01	1820	–1476	2.1	28.3	1.4	35	16.63	53	34	37
LP586–51	01 02 07.181	–00 33 01.82	2002.9	18.18	350	–118	3.6	(2.4)	2.7	—	—	47	24	120
WD0135–039	01 35 33.685	–03 57 17.90	2002.9	19.68	456	–180	3.4	13.3	2.9	75	15.26	82	21	146
LP588–37	01 42 20.770	–01 23 51.38	2002.9	*18.50	112	–328	3.4	(1.4)	4.5	—	—	57	17	120
LHS147	01 48 09.120	–17 12 14.08	2002.9	17.62	–115	–1094	2.1	14.8	1.8	68	13.46	43	29	71

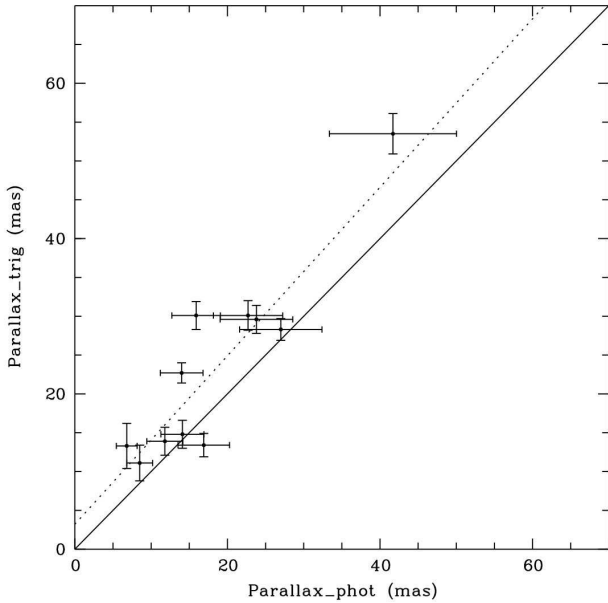


Fig. 2. Comparison of parallaxes derived in this work with photometric parallaxes from OHDHS (errors are assumed 20% for π_{phot}). Parameters of a weighted linear regression (diagonal line) between both types of parallaxes are $\pi = 1.08\pi_{phot} + 3.21$ [mas] with a reduced $\chi^2 = 8.06$. The photometric distances are systematically larger than the astrometric ones.

4.3. Proper Motions

We have compared the proper motions derived here with the OHDHS proper motions in order to check whether some systematic effects could affect our proper motions derived on a 1.5 yr

time span and, as a result, our parallaxes. We present this comparison in Fig. 3 and Fig. 4. Error bars are drawn in both coordinates but since the present work has much higher precision than the photographic astrometry, the error bars in x are not visible. The slope of a linear regression between proper motions in $\alpha \cos(\delta)$ derived in this work with the OHDHS proper motions is 1.04 ± 0.02 with a reduced $\chi^2 = 3.7$. The equivalent linear fit in proper motions in Declination has a slope of 1.01 ± 0.02 with a reduced $\chi^2 = 0.7$. For F351–50 (the largest error bars in both figures), the accordance in RA and Dec proper motions is not good. This is due to a known problem of contamination by a background galaxy of the Schmidt plate measurements used in the OHDHS work. Nevertheless the accordance is within 2σ . These comparisons show excellent agreement between both sets of proper motions, and argue against any systematic effects from the present work.

4.4. Space Velocities

We derived the Galactic space velocities U, V, W (Johnson and Soderblom 1987) for the white dwarfs using the distances and proper motions measured here together with radial velocities from Salim et al. 2004 (data available for 9 of the 15 white dwarfs treated here). Salim’s observed radial velocities were corrected for a mean gravitational redshift of +28 km/s as suggested by the authors in their paper except in the case of the very massive white dwarf LHS4033 where the correction was taken from Dahn et al. 2004. U is radial toward the Galactic center, V is in the direction of rotation and W perpendicular to the Galactic disk. U, V and W were corrected for the Sun’s peculiar velocity (Mihalas and Binney (1981)). When no radial velocity was available from other studies, we assumed $V_r = 0$ km/s. This approximation is acceptable due to its minor impact on U, V velocities since the targets are located

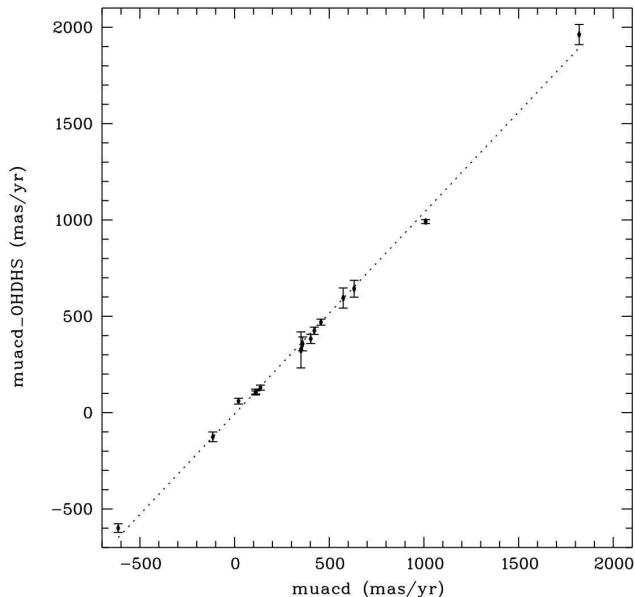


Fig. 3. Comparison of proper motions in RA $\cos(\delta)$ with the OHDHS proper motions. Error bars are drawn in both coordinates but since the present work has much higher precision than the photographic astrometry, error bars in abscissae are not visible. The slope of a linear regression (dotted line) is 1.04 ± 0.02 indicating good accordance between both proper motion data sets with a reduced $\chi^2 = 3.7$.

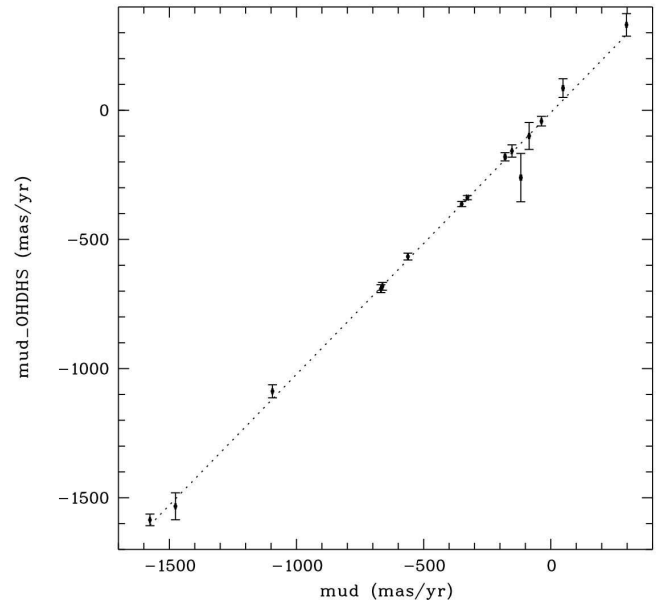


Fig. 4. Comparison of proper motions in Declination derived in this work with the OHDHS proper motions. Error bars are drawn in both coordinates but since the present work has much higher precision than the photographic astrometry, error bars in abscissae are not visible. The slope of a linear regression (dotted line) is 1.01 ± 0.02 indicating a good accordance between both proper motion data sets with a reduced $\chi^2 = 0.7$.

close to South Galactic Cap (the effect was investigated in OHDHS and shown to be negligible).

We present in Figure 5 the distribution of velocities in the Galactic plane together with the velocity dispersion for the disk (right most)(1, 2 and 3 σ), thick disk (middle)(1, 2 and 3 σ) (Fuhrmann 2004) and halo (left) (1 and 2 σ) (Chiba and Beers 2000) and in Figure 6 the component of motion perpendicular to the Galactic plane. These two figures concern the 11 objects with parallax measured at the 4 σ level or better.

In Fig. 5 one notices that 4 of the 11 studied WDs have a velocity incompatible at the 3 σ level with the kinematic of the disk and of the thick disk and that 6 of them are incompatible at a 2 σ level. No star lies within the 1 σ ellipse of the disk, primarily because of selection effects in the original proper motion survey that OHDHS based is based upon Hambly et al. 2005.

Obviously the choice of the center and dispersions of halo, thick disk and disk ellipses is critical to classify objects as belonging to a particular population. We adopted recent values which are in the range of the values cited by Reid 2005 in his review: Disk (Fuhrmann 2004) : (U,V) = (7.7, -18.1) km/s, (σ_U, σ_V) = (42.6, 22.6) km/s; thick disk (Fuhrmann 2004): (U, V) = (-18, -63) km/s, (σ_U, σ_V) = (58, 41) km/s; halo (Chiba and Beers 2000): (U,V) = (0, -180) km/s, (σ_U, σ_V) = (141, 106) km/s.

5. Discussion

As discussed above, OHDHS sparked a lively debate about whether stellar remnants contribute to a significant fraction of the baryonic component of the putative dark matter halo of our Galaxy. The main criticisms have concerned interpretation, and we do not address those here. However, the photographic pho-

tometry and use of a single photometric parallax relation are also potential sources of systematic error. Both Salim et al. (2004) and Bergeron et al. (2005) have shown that the original photometry presented in OHDHS was as accurate as could be expected. Here, we address the question of the accuracy of photometric parallaxes directly via trigonometric determination of distances.

In Fig. 2 we compare the trigonometric parallaxes derived here with the OHDHS photometric parallaxes. Parameters of a weighted linear regression between both types of parallaxes are $\pi = 1.08 \pi_{phot} + 3.21$ with a reduced $\chi^2 = 8.06$. A clear underestimation of photometric parallaxes is visible in this figure with only one point below the diagonal and three points more than 3 σ above the relation. With the usual caveat of small number statistics, this indicates some level of non-Gaussian scatter, or at least a mean value for the relation that is not coincident with $\pi = \pi_{phot}$. The photometric parallax overestimates the distance. This leads, of course, to an overestimation of tangential space velocities based on proper motion and distance (as an aside, we note that the quoted photometric parallax errors of 20% were conservatively overestimated by OHDHS).

It is interesting to note that the mass distribution of hot ($T_{\text{eff}} > 12,000$ K) DA WDs is not Gaussian and has a broad tail on the high mass side (Nalezyty et al. 2005). Given that radius $r \propto m^{-1/3}$ for WDs, we would expect photometric parallaxes to tend to overestimate rather than underestimate distances since some of the sample may have higher than average mass, and correspondingly smaller radii, placing them nearer to the Sun than typical objects of the same colour. Adding in a sprinkling of higher mass WDs with helium-dominated atmospheres will introduce further systematic overestimation of distances. It is almost certainly the case that the discrepant photometric parallaxes for WD2259-465 and WD0135-039 are caused by these effects; indeed, this has been shown to be the case for LHS 4033

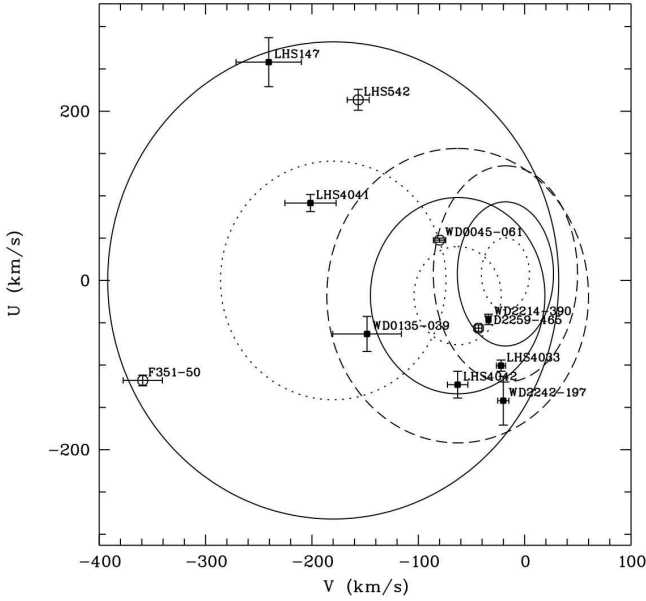


Fig. 5. Distribution of velocities in the Galactic plane together with the velocity dispersion for the disk (right most)(1, 2 and 3 σ), thick disk (middle)(1, 2 and 3 σ) (Fuhrmann 2004) and halo (left) (1 and 2 σ) (Chiba and Beers 2000). Filled squares correspond to objects with a measured radial velocity (Salim et al. 2004) while open circles correspond to objects with no V_r measurement. Only objects with parallax measured at the 4 σ level or better are plotted.

which has a mass $m \sim 1.3 M_{\odot}$ (Dahn et al. 2004). On the other hand, the low-mass side of the mass distribution is by no means perfectly Gaussian (e.g. due to low-mass, helium-core white dwarfs formed in close binaries). Moreover, any overestimation in distance leads to a corresponding underestimate of space density using the $1/V_{\max}$ technique. So the interpretation of the results from this relatively small sub-sample is rather complicated, and it is only through detailed simulations compared with much larger samples that significant progress is likely to be made concerning the question of the kinematic population of such objects.

From the comparison of trigonometric and photometric parallaxes (Fig. 2) we recalibrated photometric distances of the original OHDHS sample and, using radial velocities from Salim et al. 2004, we derived their associated recalibrated space velocities. We present the recalibrated UV plane for the entire OHDHS sample in Fig. 7.

When compared to Fig. 3 of OHDHS, the number of halo objects has diminished. From the 38 original OHDHS halo candidates, 16 appear compatible with a halo status based on a 2σ cut with the disk and thick disk velocity distributions (a 3σ cut would reduce this number to 7), the remaining objects being now located within the disk and thick disk 2 sigma ellipses. In the literature there is a large spread of the proposed values to characterise the thick disk and halo populations in terms of kinematics. For instance in Reid 2005 the velocity dispersions for thick disk vary from 50 to 69 km/s in the U direction and from 39 to 58 km/s in the V direction. Even the center of velocity ellipsoid varies from -30 to -63 km/s in the $\langle V \rangle$ coordinate from one author to another. All this makes it very difficult to separate objects into halo and thick disk populations and requires a more detailed analysis which is beyond the scope of the present paper.

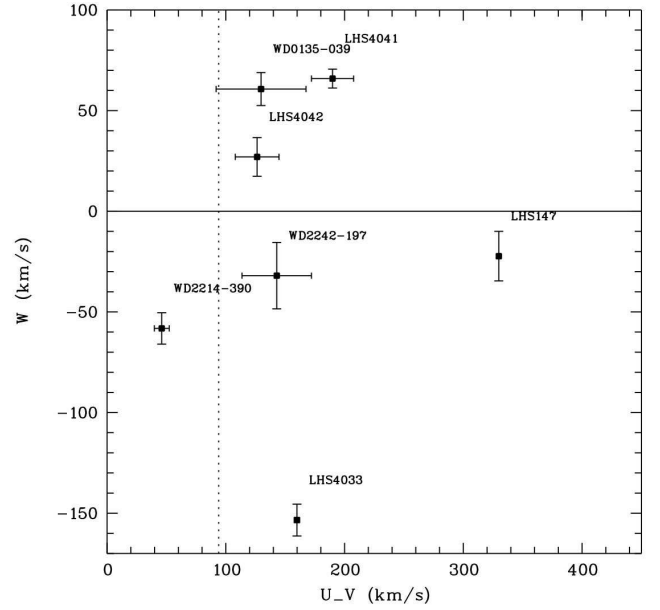


Fig. 6. Component of motion perpendicular to the Galactic plane (W) as function of $\sqrt{U^2 + V^2}$. Only objects with parallax measured at the 4 σ level or better and with available radial velocity (Salim et al. 2004) are plotted. The vertical line is the OHDHS $\sqrt{U^2 + V^2} = 94$ km/s cut.

The conclusions of OHDHS about local halo WD density must be now reanalysed since the volume explored by their survey has changed (re-calibrated distances) and the number of halo candidates has also changed. This will be the subject of a forthcoming paper.

6. Acknowledgements

The authors wish to thank G. Daigne for helpful comments and CAPES/COFECUB, FAPESP organizations and INR for supporting the project.

References

- Alcock, C. et al. 1999, in ASP Conf. Ser. 165, The third Stromlo Symposium: the Galactic Halo, ed. B.K. Gibson, T.S. Axelrod and M.E. Putman (San Francisco:ASP), 362
- Bergeron, P., Leggett, S. K. 2002, ApJ, 580, 1070
- Bergeron, P. 2003, ApJ, 586, 201
- Bergeron, P.; Ruiz, M.-T.; Hamuy, M.; Leggett, S. K.; Currie, M. J.; Lajoie, C.-P.; Dufour, P. 2005, ApJ, 625, 838
- Calchi Novati, S. et al. 2005, A&A, 443, 911
- Chabrier G., Segretain L. and Mira D., 1996, ApJ, 468, L21-L24
- Chiba, M., and Beers, T.C., 2000, AJ, 119, 2843
- Crézé, M., Mohan, V., Robin, A. C., Reylé, C., McCracken, H. J., Cuillandre, J.-C., Le Fèvre, O., Mellier, Y., 2004, A&A, 426, 65
- Cutri R. M., Skrutskie M. F., Van Dyk S. et al., 2003
- Dahn, C. C., Bergeron, P., Liebert, J., Harris, H. C., Canzian, B., Leggett, S. K., Boudreault, S. 2004, ApJ, 605, 400
- Davies, M. B., King, A. R., Ritter, H. 2002, MNRAS, 333, 469
- Eichhorn, H. and Williams, C.A. 1963, AJ, 68, 221
- Eichhorn, H. 1997, Astron. Astrophys., 327, 404
- Flynn, C., Holopainen, J., Holmberg, J., 2003, MNRAS, 339, 817
- Fuhrmann K. 2004, Astron. Nact. 325:3-80
- Gates, E. et al. 2004, ApJ, 612, 129L
- Hansen, B. M. S., 1998, Nature, 394, 860
- Hansen, B. M. S. 2003, ApJ, 582, 915
- Hansen, B. M. S. and Liebert, J. 2003, ARA&A, 41, 465
- Hambly, N. C., Digby, A. P., Oppenheimer, B. R., 2005, ASPC, 334, 113

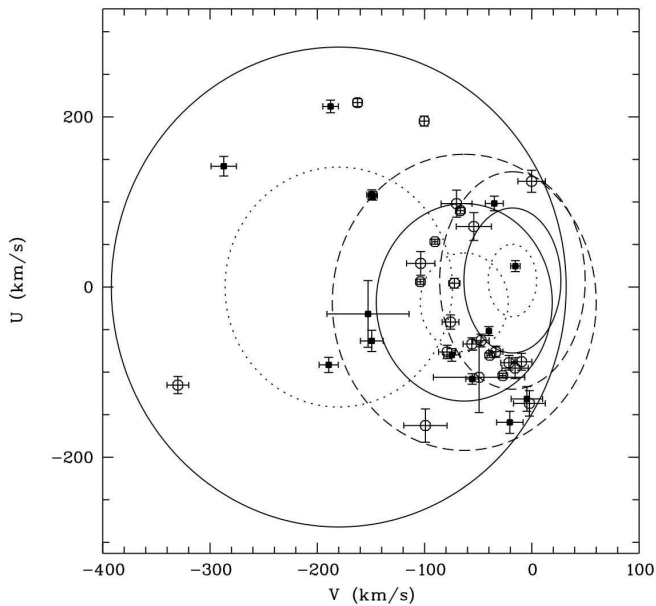


Fig. 7. Distribution of velocities of the original OHDHS sample with recalibrated parallaxes in the Galactic plane together with the velocity dispersion for the disk (right most) (1, 2 and 3 σ), thick disk (middle) (1, 2 and 3 σ) (Fuhrmann 2004) and halo (left) (1 and 2 σ) (Chiba and Beers 2000). Filled squares correspond to objects with a measured radial velocity (Salim et al. 2004) while open circles correspond to objects with no V_r measurement.

- Hawkins, M. R. S., Ducourant, C., Jones, H. R. A. and Rapaport, M., 1998, MNRAS, 294, 505
 Holopainen, J., Flynn, C., 2004, MNRAS, 351, 721
 Johnson, D. R. H., Soderblom, D. R. 1987, AJ, 93, 864
 Kilic, M., Mendez, R. A., von Hippel, T., Winget, D. E., 2005, ApJ, 633, 1126
 Kowalski, P. M. 2006, ApJ, 641, 488
 Nalezyty, M., Madej, J., Althaus, L. G. 2005, ASPC 334, 107
 Mihalas, D., Binney, J. 1981, "Galactic astronomy", second edition.
 Monet D.G., Dahn C.C., Vrba F.J., Harris H.C., Pier J.R., Luginbuhl C.B., Ables H.D., 1992, AJ, 103, 638
 Montiero, H., Jao, W.-C., Henry, T., Subasavage, J., Beaulieu, T. 2006, ApJ, 638, 446
 Oppenheimer, B. R., Hambly, N. C., Digby, A. P., Hodgkin, S. T., Saumon, D. 2001, Science, 292, 698 (OHDHS)
 Reid, I. N., 2005, ARA&A, 43, 247
 Robin, A., 1994, ApSS, 217, 163R
 Salim, S., Rich, R. M., Hansen, B. M., Koopmans, L. V. E., Oppenheimer, B. R., Blandford, R. D., 2004, ApJ, 601, 1075
 Torres, S., García-Berro, E., Burket, A., Isern, J. 2002, MNRAS, 336, 971
 Saumon, D.; Jacobson, S. B. 1999, ApJ, 511, L107
 Silvestri, N. M., Oswalt, T. D., Hawley, S. L. 2002, AJ, 124, 1118
 Spagna, A., Carollo, D., Lattanzi, M. G., Bucciarelli, B. 2004, A&A, 428, 451
 Stetson Peter B., 1987, PASP, 99, 191
 Van Altena, W. F., Lee J. T., Hoffleit E. D. 1995, General Catalogue of Trigonometric Stellar Parallaxes, Fourth Edition, Yale University Observatory

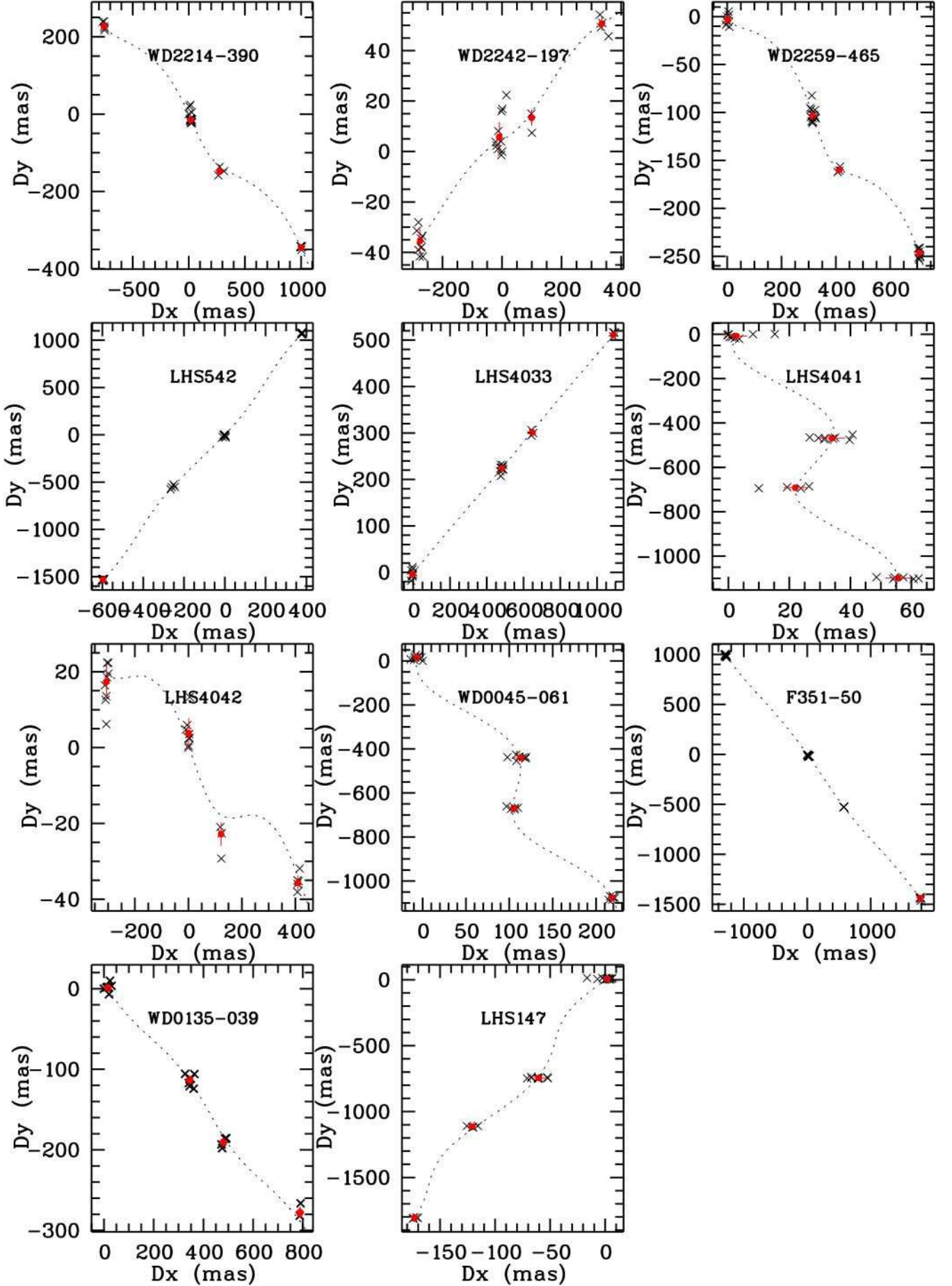


Fig. 8. Observations along the fitted path expressed in mas.